Journal of Zhejiang University-SCIENCE A (Applied Physics & Engineering)
ISSN 1673-565X (Print); ISSN 1862-1775 (Online)
www.jzus.zju.edu.cn; www.springerlink.com
E-mail: jzus@zju.edu.cn

A simplified nonlinear calculation method to describe the settlement of pre-bored grouting planted nodular piles*

Jia-jin ZHOU[1,2], Xiao-nan GONG[†‡1,2], Kui-hua WANG[1,2], Ri-hong ZHANG[3], Jia-jia YAN[1,2]

([1]*Research Center of Coastal and Urban Geotechnical Engineering, Zhejiang University, Hangzhou 310058, China*)

([2]*MOE Key Laboratory of Soft Soils and Geoenvironmental Engineering, Zhejiang University, Hangzhou 310058, China*)

([3]*ZCONE High-tech Pile Industry Holdings Co., Ltd., Ningbo 315000, China*)

[†]E-mail: xngong@hzcnc.com

Received Sept. 28, 2016; Revision accepted May 16, 2017; Crosschecked Oct. 11, 2017

Abstract: The pre-bored grouting planted nodular (PGPN) pile is a type of composite pile foundation that is considered to be environmentally friendly and economical. A simplified approach, which considers the two interfaces of the pile shaft, was proposed to analyze the load-displacement response of a single PGPN pile. An elastic-failure model, based on the shear test results, was used to simulate the shearing behavior of the concrete-cemented soil interface. A hyperbolic nonlinear model, considering the influence of cement paste injection, was created to simulate the behavior between the skin friction and the relative displacement developed along the cemented soil-soil interface. A linear model and a nonlinear model that considers the reduction in the shearing stiffness were used to simulate the PGPN pile base load-displacement responses in a field test and in a model test, respectively. Comparisons between the calculated and measured load-displacement responses revealed relatively good agreement. The proposed approach is thus shown to be efficient and suitable for the analysis of a single PGPN pile embedded in layered soils, and is used to analyze the factors influencing its behavior. Enlarged cemented soil base is considered to be effective in promoting the behavior of a short PGPN pile, while increasing the diameter of cemented soil along the shaft is efficient in promoting the compressive bearing capacity of a long PGPN pile.

Key words: Composite pile; Precast pile-cemented soil-surrounding soil interface; Initial shearing stiffness of pile-soil interface; Elastic-failure model; Hyperbolic nonlinear model; Settlement calculation

http://dx.doi.org/10.1631/jzus.A1600640 **CLC number:** O324

1 Introduction

A number of studies have been conducted to investigate the behavior of single piles and pile groups under compression. Randolph and Wroth (1978; 1979) proposed a simplified analytical method to describe the vertical deformation of single piles and pile groups. Frank and Zhao (1982) proposed an effective approach for the analysis of pile foundation. The theoretical load-transfer curve method is commonly used to analyze the behavior of piles (Kraft *et al*., 1981). The boundary element and finite element methods have also been used to study the behavior of piles (Mandolini and Viggiani, 1997; Sheng *et al*., 2005; Ai and Han, 2009; Comodromos *et al*., 2009; Said *et al*., 2009).

The theoretical methods mentioned above are all important in the analysis of the behavior of driven piles and bored piles. However, the construction method of driven piles tends to produce severe

‡ Corresponding author

* Project supported by the National Natural Science Foundation of China (Nos. 51578498 and 51579217), the Science and Technology Plan Program of Ningbo, China (No. 2013B81003), the China Postdoctoral Science Foundation (No. 2017M611995), the Open Funding of the Key Laboratory of Geotechnical and Underground Engineering, Ministry of Education, China (No. KLE-TJGE-B1501)

ORCID: Jia-jin ZHOU, http://orcid.org/0000-0003-4267-1454; Xiao-nan GONG, http://orcid.org/0000-0001-5218-5324

© Zhejiang University and Springer-Verlag GmbH Germany 2017

compaction and may have a negative effect on surrounding facilities, while the construction process of bored piles tends to produce large amounts of slurry, which may bring serious environment problems. Moreover, the skin friction provided by the surrounding soil is relatively small in soft soil areas, and the ultimate bearing capacity of the pile is primarily controlled by the pile head settlement; therefore, the strength of the pile shaft is not always fully mobilized, which is not typically economical. As a result, several advanced piles have been developed, particularly with regard to the load transfer mechanism of pile foundation. The pre-bored grouting planted nodular (PGPN) pile is a composite pile consisting of a precast nodular pile and cemented soil surrounding it. Its diameter ranges from 500 mm to 1000 mm, while its length can reach 80 m. The nodular pile was first used in Japan, and several Japanese scholars have investigated its behavior (Horiguchi and Karkee, 1995; Karkee *et al*., 1998). The PGPN pile has also been used in some soft soil areas in southeastern China in recent years. The behavior of PGPN pile was investigated based on measured data from field tests and model tests (called the static drill rooted planted pile in these papers) (Zhou *et al*., 2013; 2015; 2016), and the test results showed that the frictional capacity of PGPN piles is better than the frictional capacity of bored piles.

A PGPN pile shaft contains the precast concrete pile-cemented soil interface and the cemented soil-soil interface, and the frictional capacity of PGPN piles is different from that of conventional concrete piles. Therefore, the theoretical methods proposed to analyze the behavior of driven piles and bored piles may not be suitable for the analysis of PGPN piles. This paper presents a simplified analytical approach, which is based on the well-known load-transfer approach, for the nonlinear analysis of the load-displacement response of a PGPN pile using different models. One model is based on the shear test results and approximately simulates the behavior of the concrete-cemented soil interface. The other model is based on a hyperbolic relationship and describes the nonlinear response of the skin friction supported by the surrounding soil. The parameters of the adopted model should be modified based on the original values of a conventional concrete pile. A linear model and a nonlinear model that considers the reduction in the shearing stiffness were selected to simulate the pile tip load-displacement response in two tests. Moreover, an effective computer program was built for the nonlinear analysis of the load-displacement response of a PGPN pile. The results of the two tests presented here demonstrate the efficiency and accuracy of the proposed approach and also reveal the advantages of the PGPN pile.

2 Concrete-cemented soil interface shear test

The PGPN pile installation process is introduced in a previous study (Zhou *et al*., 2013), and the schematic of the PGPN pile is depicted in Fig. 1 (Zhou *et al*., 2017). This figure shows that the PGPN pile consists of a precast pile and the surrounding cemented soil. Moreover, Fig. 1 shows that the pipe pile and nodular pile are used jointly in actual projects by considering the load transfer mechanism of the pile foundation.

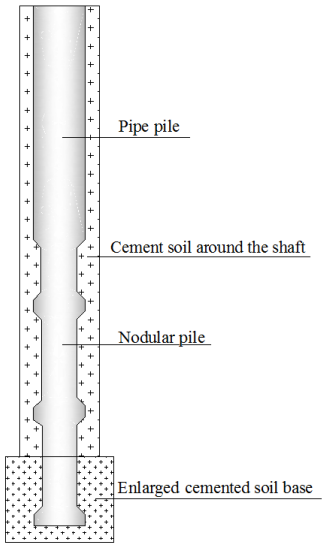

Fig. 1 Schematic of the PGPN pile (Reprinted from (Zhou *et al*., 2017), Copyright 2017, with permission from Springer)

For example, an 800-mm prestressed high strength concrete pile is typically connected to an 800 (600)-mm nodular pile (i.e., the diameter of the pile node is 800 mm, while the pile shaft has a diameter of 600 mm). It is commonly acknowledged that the

axial force of the pile shaft decreases as the load is transferred to the surrounding soil. Moreover, the strength of the lower part of the pile shaft is typically lower than that of the upper part in an optimal design. Therefore, the combination of a pipe pile and a nodular pile can provide better performance compared with conventional uniform piles.

The cemented soil around the pile can increase the pile shaft diameter and eventually increase the bearing capacity of the pile foundation. It can be seen from Fig. 1 that the frictional capacity of the precast pile-cemented soil interface is of great significance for the behavior of PGPN pile, yet no research has ever been conducted to study the shearing behavior of the concrete-cemented soil interface. Therefore, an interface shear test was conducted to investigate the frictional capacity of the concrete-cemented soil interface.

2.1 Shear test preparation

The shear test was conducted in a specific apparatus, as shown in Fig. 2 (Zhou *et al*., 2017), to ensure the shearing surface was similar to the actual shearing surface of the pile-cemented soil interface. It can be seen from Fig. 2 that the model concrete pile and cemented soil were located at the middle of the shear test apparatus, surrounded by sandy soil. The diameter of the shear apparatus was 900 mm and the diameter of the concrete pile segment and cemented soil were 90 mm and 160 mm, respectively. The distance between the concrete pile segment and the edge of the test apparatus reached 5 times the pile diameter.

Fig. 2 Shear test apparatus (Reprinted from (Zhou *et al*., 2017), Copyright 2017, with permission from Springer)

The cemented soil used in the shear test was produced by typical Ningbo clayey soil and P.O. 42.5 cement, and the ratio of the cemented soil was determined according to that used in the actual projects. That is, the water cement ratio of the cement paste was 1.0, and the volumetric ratio of the cement paste and slurry (50% water content) was 0.5. The precast concrete pile segment was made by C80 concrete (the strength of the 100 mm×100 mm×100 mm concrete sample reaches 80 MPa after being cured for 28 d). The surface of the pile segment was as smooth as the actual pipe pile, as shown in Fig. 3.

The surrounding sandy soil was "concrete sand", that is, the sand was used for producing concrete. The grading curve of the sandy soil is shown in Fig. 4 and it can be seen that the sand has good grain composition.

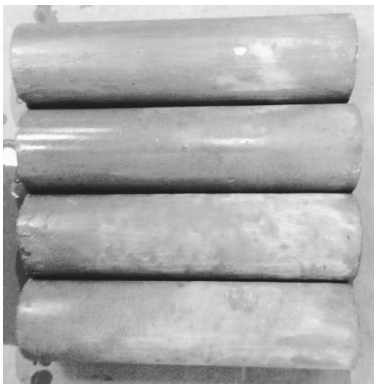

Fig. 3 Precast concrete pile segment

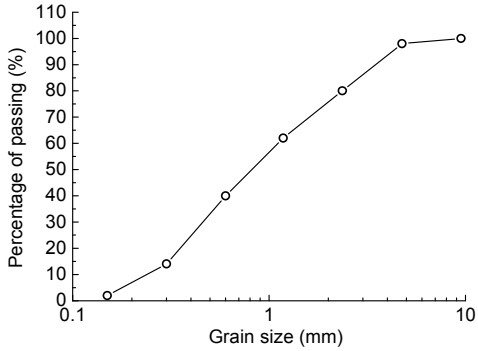

Fig. 4 Grading curve of the sandy soil

The sandy soil was filled layer by layer, and the thickness of one layer was 0.05 m after compaction. The homogeneity of the sandy soil was examined after each soil layer was compacted to the set line, and soil samples obtained from three different places with cutting rings were tested. The average density of the

samples should not deviate over 5% of the given value; moreover, the density of any two samples should also not deviate over 5% of the given density. Conventional laboratory tests were conducted when the sandy soil was compacted to the desired density and saturated completely. The sandy soil could be considered as normally consolidated soil. The density of the sandy soil was 2300 kg/m^3 using the cutting ring method. The peak internal friction angle and cohesion of the sandy soil were 38° and 0 kPa, respectively, measured by conventional direct shear tests.

2.2 Interface shear test

The shear test was conducted after the cemented soil being cured for 28 d, and the test was loaded by a 100 kN hydraulic jack. The applied load was measured by a matched pressure sensor which had a digital display device, and the pressure sensor had been calibrated in a standard calibration facility. The displacement of the pile segment was measured using a dial gauge. During the shear test, concrete blocks were also put on the test apparatus to restrict movement of the cemented soil and sandy soil. The schematic of the shear test is presented in Fig. 5 (Zhou *et al*., 2017). The measured pile segment displacement can be taken as the shear displacement of the concrete-cemented soil interface.

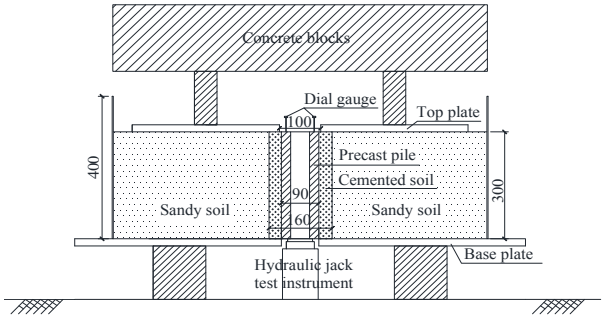

Fig. 5 Schematic of the shear test (unit: mm) (Reprinted from (Zhou *et al*., 2017), Copyright 2017, with permission from Springer)

2.3 Test results analysis

Three repeated tests were conducted to ensure the reliability of the test results. The test results are presented in Fig. 6, and the failure surface of the concrete-cemented soil interface is shown in Fig. 7. Fig. 7 shows that the failure occurred just at the contact surface of the concrete and cemented soil, and the failure surface was as smooth as the concrete pile surface. Fig. 6 shows that the three shear tests all achieved the maximum values with 1.09 mm, 1.40 mm, and 1.37 mm shear displacements and that the maximum values were 189 kN, 189 kN, and 200 kN, respectively. Hence, the pile-cemented soil interface achieved the maximum value when the shear displacement reached 1.4% of the pile diameter. Fig. 6 also shows that abrupt failure occurred when the friction reached the ultimate value, and a clear sound could be heard when the abrupt failure happened. It should be pointed out that the residual skin friction values for the interface were all approximately 20 kPa, while the shear displacement of the interface was much larger than 10 mm (denoted as 10 mm in Fig. 6).

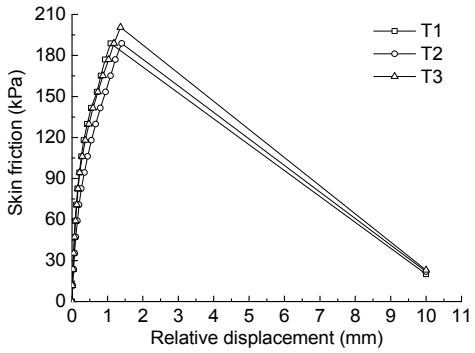

Fig. 6 Results of the three shear tests (T1, T2, and T3)

Fig. 7 Failure surface of the shear test

The cohesion and internal frictional angle of the cemented soil were 193 kPa and 38°, respectively. The overburden pressure on the sandy soil, as shown in Fig. 5, was approximately 100 kPa. The at-rest earth pressure coefficient K_0 could be estimated based on the effective angle of shearing resistance (K_0=

1−sinφ, where φ is the internal friction angle of the sandy soil), and K_0 was about 0.38. Kulhawy (1984) pointed out that, for smooth concrete pile, the frictional angle of the pile-soil interface is 0.8–1.0 times that of the internal frictional angle of the surrounding soil. The frictional angle of the pile-cemented soil interface was therefore assumed to be 0.8 times that of the internal fictional angle of the cemented soil.

The ultimate skin friction of the concrete-cemented soil interface f_{su}, based on the properties of the cemented soil, was calculated by

$$f_{su} = c + K_0\sigma_{v0}\tan\beta, \tag{1}$$

where c is the cohesion, β is the frictional angle of the interface, and σ_{v0} is the vertical effective stress.

The calculated ultimate skin friction, if using the cohesion of the cemented soil, was 215 kPa, which is close to the measured values. Hence, it can be considered that the frictional capacity of the concrete-cemented soil interface is mainly controlled by the properties of the cemented soil. Moreover, the initial cohesion takes a majority part of the entire skin friction.

As a result, considering that the residual skin friction of the concrete-cemented soil interface after failure was fairly limited (20 kPa), an elastic-failure model was adopted to simulate the behavior of the concrete-cemented soil interface (Fig. 8).

The value of S_{ru} was set as 1.4% of the pile diameter, and the ultimate skin friction f_{su} was calculated by Eq. (1). The test results also indicated that the ultimate skin friction of the concrete-cemented soil interface was much larger than that of the cemented soil-soil interface.

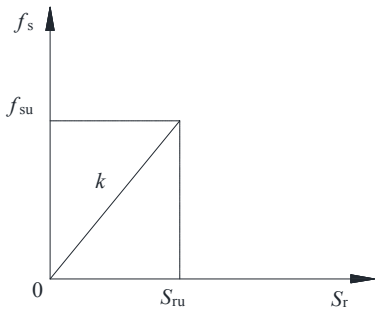

Fig. 8 Assumed linear relationship between friction (f_s) and relative displacement (S_r) of concrete-cemented soil interface (k=f_{su}/S_{ru})

3 Hyperbolic nonlinear model

3.1 Description of the hyperbolic nonlinear model

Kondner (1963), Duncan and Chang (1970), and Frank and Zhao (1982) showed that the hyperbolic nonlinear model can be used to effectively simulate the nonlinear stress-strain behavior of both clay and sand with accurate experimental parameters. The hyperbolic nonlinear model is also used for the analysis of the nonlinear behavior of cemented soil-soil interface in the PGPN pile system, as shown in Fig. 9.

Fig. 9 shows that the skin friction increases nonlinearly with the relative displacement between the pile and the soil and nearly achieves its highest value p_{su} when the pile-soil relative displacement reaches S_{su}. This hyperbolic relationship can also be approximately expressed by

$$p_s(z) = \frac{S_s(z)}{a + bS_s(z)}, \tag{2}$$

where $p_s(z)$ is the pile shaft shear stress at a given depth z, $S_s(z)$ is the pile-soil relative displacement, and a and b are empirical coefficients, which are always determined by back-analysis of the field test results.

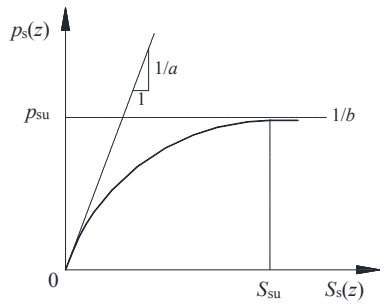

Fig. 9 Assumed relationship between skin friction and the relative displacement between the pile and the soil

3.2 Determination of the parameters *a* and *b*

As mentioned in Section 3.1, the parameters a and b are empirical coefficients that both have an effect on the shape of the hyperbolic curve. Therefore, it is important to choose suitable values for a and b. Fig. 9 shows that the reciprocal of coefficient a can be considered to be the initial stiffness of the pile-soil interface. Randolph and Wroth (1978) proposed an

equation to calculate the value of a for driven piles and bored piles:

$$a=\frac{r_0}{G_s}\ln\left(\frac{r_m}{r_0}\right), \tag{3}$$

where G_s is the shear modulus of the soil around the shaft, r_0 is the radius of the pile, and r_m is the distance from the pile's central axis to the place where the shear stress induced by the pile can be ignored. The value of r_m can be obtained by

$$r_m=2.5L(1-0.5\mu), \tag{4}$$

where L is the entire length of the pile, and μ is Poisson's ratio of the soil around the shaft. The initial shear modulus of the soil can be approximately calculated by the following theoretical equation:

$$G_s=\frac{E_s}{2(1+\mu)}, \tag{5}$$

where E_s is the elastic modulus of the soil around the pile.

As mentioned above, the PGPN pile is a composite pile consisting of a precast pile and cemented soil surrounding it. Hence, there are four radii for the composite pile: r_0 is the radius of the composite pile (i.e., the radius of the cemented soil), r_p is the radius of the pipe pile, r_n is the radius of the nodular pile shaft, and r_b is the radius of the enlarged cemented soil base. As mentioned in a previous study, the precast pile and the surrounding cemented soil can be considered to be one system during the load transfer process, and the cemented soil acts as a transition layer in which the stress is relatively small (Zhou *et al*., 2013). The choice of the radius may affect the calculation result of the composite pile, and the test results of this study will be used to help determine a suitable radius.

It can also be seen in Fig. 9 that the reciprocal of parameter b is the asymptote of the pile shaft stress-relative displacement curve. The asymptote shaft shear strength p_{su} is shown to be marginally larger than the maximum possible value of the pile-soil interface p_u; a failure ratio R_f is used to describe the relationship between p_{su} and p_u:

$$b=\frac{1}{p_{su}}=\frac{R_f}{p_u}. \tag{6}$$

The failure ratio R_f represents the ratio between the maximum possible skin friction and the asymptotic value of the highest skin friction, and the values of R_f are commonly in the range of 0.80–0.95 (Clough and Duncan, 1971).

The test results of an accurate model of a single PGPN pile, which was introduced in a previous study (Zhou *et al*., 2015), were adopted in this study to help determine the parameters of the hyperbolic model. The soil profiles and properties are shown in Table 1, where γ is the unit weight of the soil.

The model PGPN pile was a 90 (60)-mm nodular pile with a length of 2 m, and the diameter of the surrounding cemented soil was 110 mm. The diameter of the enlarged cemented soil base was 165 mm and its height was 330 mm. The soil around the model pile was mainly clay, and the base soil was a 0.5-m thick sand layer. The schematic of the model test is shown in Fig. 10.

The measured ultimate skin friction was used to help determine the parameters of the hyperbolic model and calculate the load-displacement response for the PGPN pile. Parameter a was calculated based on Eqs. (3) and (4), and the comparisons between the measured skin frictions and the fitted results are shown in Fig. 11.

Fig. 11a shows the comparative results of the upper three clay soil layers. The radius of the PGPN pile r_0 was 55 mm, and the radius of the nodular pile r_n was 30 mm. It is shown in Fig. 11a that the hyperbolic model used with the selected parameters displayed relatively good agreement with the measured results when the failure ratio R_f was equal to 1.0, 0.95, and 0.95 from shallow to deep; moreover, the selection of the radius has little influence on the fitted curve.

Table 1 Soil profiles and properties in model test

Layer No.	Soil layer	Soil layer thickness (m)	γ (kN/m^3)	φ (°)	c (kPa)	μ	E_s (MPa)	G_s (MPa)
1	Clay	1.8	19.10	30.5	24.5	0.30	5.35	2.06
2	Sand	0.7	19.92	35.0	0	0.25	15.80	6.32

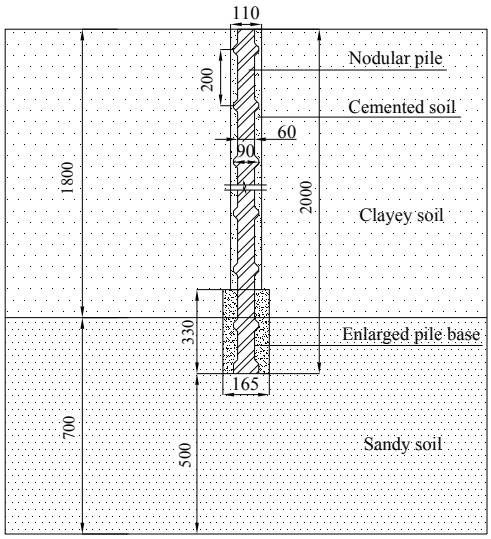

Fig. 10 Schematic of the model test (unit: mm)

Fig. 11b shows the comparisons between the measured results and simulated results for the three clay soil layers from depths of 0.6 m to 1.4 m. The proposed hyperbolic model also fits well with the measured results when the initial shearing stiffness of the pile-soil interface is multiplied by 2.0, 3.5, and 3.5 from shallow to deep. The failure ratio R_f was 0.95 for all three soil layers. The increase in the initial shearing stiffness was primarily because of the injection of cemented soil which promotes the shear modulus of the pile-soil interface. Fig. 11b also shows that the radius of the pile has little influence on the shape of the fitted curve.

Fig. 11c shows the comparative results of the three soil layers from depths of 1.4 m to 2.0 m. The fitted curves represent the measured values accurately when the initial shearing stiffness of the pile-soil interface is multiplied by 5.0, 5.0, and 2.0 from shallow to deep. The failure ratio R_f was 0.95 for all three soil layers.

By combining the analyses above, the shape of the fitted curve remains almost unchanged when the two radii (r_0 and r_n) of the composite pile are chosen as the pile radius, respectively. The radius of the composite pile r_0 was selected to be the pile radius in this study because the ultimate skin friction of the concrete-cemented soil interface is much larger than that of the cemented soil-soil interface. Fig. 11 also shows that the shearing stiffness of the pile-soil interface was increased due to the permeation of the cement paste, and this improvement increases along

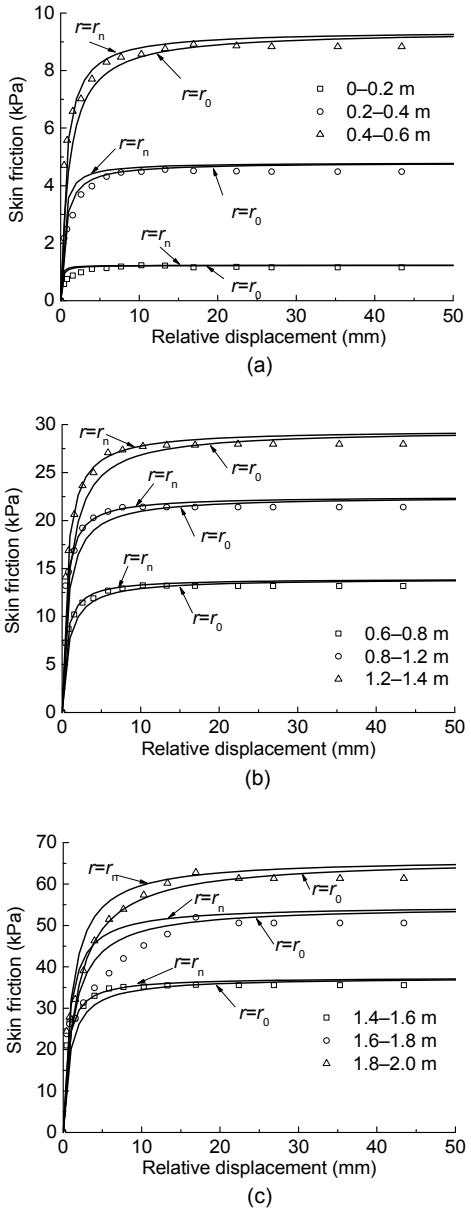

Fig. 11 Comparisons between the measured and fitted results of the skin friction as a function of the relative displacement from different depths: (a) 0–0.6 m; (b) 0.6–1.4 m; (c) 1.4–2.0 m

the pile shaft. The probable reason is that the cemented soil flows when being poured into the borehole, and the hydraulic pressure increases with depth, which increases the permeation pressure. The initial shearing stiffness of the sandy soil layer was only increased by 2.0 times, which was smaller than the upper soil layers. This is because the enlarged cemented soil base was manufactured in advance, and the permeation pressure was small (Zhou *et al*., 2015).

4 Nonlinear base load-displacement model

The hyperbolic nonlinear model is commonly used to simulate the pile base load-displacement relationship (Lee and Xiao, 2001). The behavior of PGPN pile tip in the model test is shown in Fig. 12. Fig. 12 shows that the relationship between the tip displacement and the mobilized base load is nonlinear.

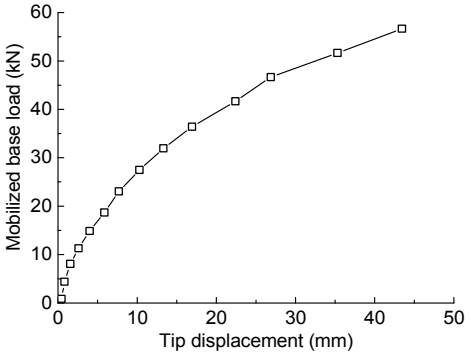

Fig. 12 Pile tip displacement as a function of the mobilized base load in the model test

The pile tip displacement induced by the mobilized base load, without regard to the change in shear modulus of base soil, can be expressed as (Randolph and Wroth, 1978)

$$S_b = \frac{P_b(1-\mu)}{4r_b G_b}, \tag{7}$$

where P_b and S_b are the tip resistance and pile base displacement, respectively, G_b is the shear modulus of the base soil, μ is Poisson's ratio of the base soil, and r_b is the radius of the pile base. Fig. 1 shows that an enlarged cemented soil base exists at the PGPN pile base, thus suggesting that the precast pile base and the enlarged cemented soil base act as a unit during the load transfer process (Zhou *et al*., 2013). The radius of the enlarged cemented soil base r_b=82.5 mm is considered to be the pile base radius of the PGPN pile.

The nonlinear behavior of the soil at pile base can be simulated by (Han and Ye, 2006)

$$G_b = G_{bi}\left(1 - R_f \frac{P_b}{Q_b}\right)^2, \tag{8}$$

where G_{bi} is the initial shear modulus of the base soil, Q_b is the maximum base load, and P_b is the mobilized base load.

The initial shear modulus of the base soil was 12 MPa (using Eq. (7)) referring to the initial portion of the curve in Fig. 12. The simulation results are shown in Fig. 13 when the failure ratio was selected to be 0.55, 0.60, and 0.65. Fig. 13 shows that the fitted curve has a relatively good relationship with the measured results when the failure ratio is 0.55. The failure ratio of the fitted curve is relatively small, which is probably due to the permeation of the cemented soil. Moreover, as shown in Table 1, the initial shear modulus of the base soil was approximately 6.3 MPa, while the measured initial shear modulus was 12 MPa. The measured initial shear modulus was increased to about 1.9 times of the initial shear modulus of the base soil, which is close to the increasing range of the initial shearing stiffness of the bottom 0.2-m sand layer. Therefore, the properties of the base soil were also promoted as the permeation of the cemented soil, and the initial shear modulus and the strength both increased.

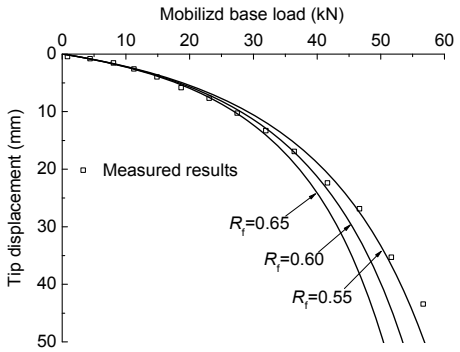

Fig. 13 Fitted curves of tip displacement as functions of the mobilized base load

5 Algorithm for the load-displacement behavior of a single PGPN pile embedded in layered soils

Based on the proposed models above, the theoretical method for a single PGPN pile embedded in layered soils can be analyzed with the following steps:

1. Consider a single PGPN pile that is divided into (m_1+m_2) segments, as shown in Fig. 14. Because the pile shaft modulus is different, the PGPN pile

shaft which contains the pipe pile is divided into m_1 segments, and the shaft which contains the nodular pile is divided into m_2 segments. Therefore, there are (m_1+m_2) segments in total. Note that the model test does not include pipe pile segments; thus, m_1 can be considered equal to 0.

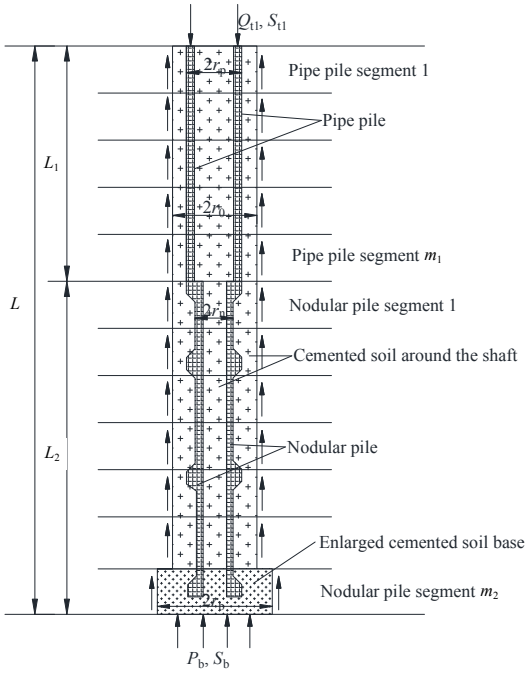

Fig. 14 A single PGPN pile embedded in layered soils
Q_{t1} is the pile head load; S_{t1} is the pile head displacement; L_1 and L_2 are the lengths of the pipe pile segment and nodular pile segment, respectively

2. Consider a small mobilized base load P_b. Calculate the tip displacement S_b using Eqs. (7) and (8). The radius of the enlarged cemented soil base r_b is considered to be the radius of the PGPN pile base in the pile base load calculation.

3. A vertical displacement at the middle height of the nodular pile segment m_2, denoted S_{m2}, is assumed to be equal to S_b.

4. The skin friction of the cemented soil-soil interface of PGPN pile segment m_2, denoted p_{sm2}, can be obtained based on the calculated displacement of PGPN pile segment m_2 using Eq. (2). The sketch of the PGPN pile shaft is shown in Fig. 15, where p_s is the skin friction of the cemented soil-soil interface, and f_s is the skin friction of the pile-cemented soil interface. The skin friction of the pile-cemented soil interface of PGPN pile segment m_2, denoted f_{sm2}, is $(r_0/r_p)p_{sm2}$. The ultimate skin friction of the pile-cemented soil interface of PGPN pile segment m_2, denoted f_{sum2}, can be calculated by Eq. (1).

The relative displacement of the pile-cemented soil interface, S_{rm2}, can be calculated by the following equation, assuming that the ultimate relative displacement is 1.4% of the pile diameter:

$$S_{rm2}=\frac{0.014df_{sm2}}{f_{sum2}}, \tag{9}$$

where d is $2r_p$ in pipe pile segment and changes to $2r_n$ in nodular pile segment. Note that the value of f_{sum2} should be larger than the value of f_{sm2} to ensure the integrity of the PGPN pile, and the calculation procedure should be terminated if $f_{sum2}<f_{sm2}$, which indicates that the pile-cemented soil interface is damaged and the PGPN pile has failed.

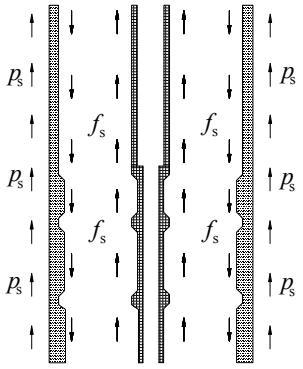

Fig. 15 Sketch of the interfaces in PGPN pile system

5. The top load of the PGPN pile segment m_2, denoted P_{tm2}, can be determined using the calculated p_{sm2} in the following equation:

$$P_{tm2}=P_b+2\pi r_0 L_{nm2}p_{sm2}, \tag{10}$$

where L_{nm2} is the length of nodular pile segment m_2.

6. Assume that the PGPN pile shaft is elastic, and a linear variation of the load occurs in the pile segment. The elastic deformation of the lower half segment of nodular pile segment m_2, denoted S_{em2}, can be calculated by

$$S_{em2}=\left(\frac{P_{tm2}+3P_{bm2}}{4}\right)\left(\frac{L_{nm2}}{2E_{p2}A_{p2}}\right), \tag{11}$$

where P_{bm2} is the tip load of the PGPN pile segment m_2, and E_{p2} and A_{p2} are the modulus and cross sectional area of the nodular pile, respectively.

Similarly, the elastic deformation of the lower half segment of pipe pile segment m_1, denoted S_{em1}, can be calculated by

$$S_{em1}=\left(\frac{P_{tm1}+3P_{bm1}}{4}\right)\left(\frac{L_{nm1}}{2E_{p1}A_{p1}}\right), \tag{12}$$

where E_{p1} and A_{p1} are the modulus and cross sectional area of the pipe pile, respectively.

7. The revised displacement at the middle height of the nodular pile segment m_2, denoted S_{rrm2}, can be determined by

$$S_{rrm2}=S_b+S_{em2}. \tag{13}$$

8. Compare the value of the revised displacement of the nodular pile segment m_2 with the assumed value of S_{m2} in step 3. If the absolute difference between S_{m2} and S_{rrm2} exceeds the specified tolerance value (e.g., 10^{-6} m in this study), the value of the revised displacement of nodular pile segment m_2 will be substituted into Eq. (2) for the calculation of the unit skin friction of the nodular pile segment m_2, denoted p_{sm2}, in step 4.

9. Repeat steps 3–8 until the absolute difference between S_{m2} and S_{rrm2} is within the specified tolerance, and a reliable displacement of nodular pile segment m_2, denoted S_{srm2}, is obtained.

10. Calculate the top load of the nodular pile segment m_2, denoted P_{tm2}, using Eq. (10). The top displacement of nodular pile segment m_2, denoted S_{tm2}, can be calculated by

$$S_{tm2}=S_b+\left(\frac{P_{tm2}+P_{bm2}}{2}\right)\left(\frac{L_{nm2}}{E_{p2}A_{p2}}\right). \tag{14}$$

11. The tip load and the tip displacement of the nodular pile segment (m_2−1) are assumed to be the same as the top load and the top displacement of nodular pile segment m_2, respectively. Repeat steps 3–10 from the nodular pile segment m_2 to the first pipe pile segment to obtain the top load and the displacement of pipe pile segment 1, before judgments are made as to whether the pile shaft is a nodular pile segment or a pipe pile segment.

12. Repeat steps 2–11 with a series of mobilized pile base loads P_b to obtain the multiple pile top load-displacement pairs. Finally, the simulated curve will be formed by the calculated load-displacement pairs.

The proposed simplified analytical approach is effective and suitable for the analysis of a single PGPN pile embedded in layered soils by considering the precast pile-cemented soil interface and the cemented soil-surrounding soil interface along the shaft. The changing pile shaft modulus along the shaft and the existence of the enlarged cemented soil base are also considered in this approach.

6 Comparison of the measured and calculated results for a single PGPN pile

6.1 Comparison of a short PGPN pile

The measured results of the PGPN piles were used to verify the reliability of the proposed algorithm for the analysis of the load-displacement response of a single PGPN pile in layered soils.

The results of the model test mentioned in Section 3 were used to verify the reliability of the proposed method. The determinations of the models and parameters are listed in Sections 3 and 4, and the comparisons between the computed and measured load-displacement curves are shown in Fig. 16. This figure shows that the calculated values fit well with the measured values, and the calculated curve can thus be considered to be reliable.

The proposed algorithm above was then used to analyze the influence of the enlarged cemented soil base on the behavior of short PGPN piles. The

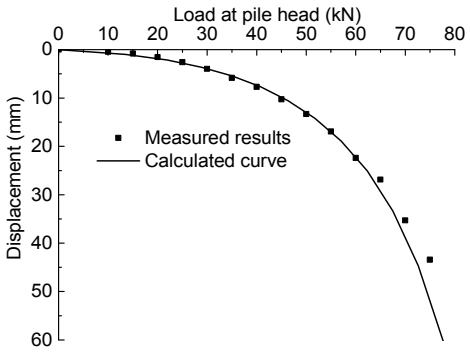

Fig. 16 Comparisons between computed and measured load-displacement response for a single PGPN pile

diameter of the enlarged cemented soil base in the model test was 165 mm, and the diameter of the pile shaft was 110 mm. The tip bearing capacity of the PGPN pile with no enlarged cemented soil base could also be approximately estimated based on the measured soil pressure of the soil under pile tip, and the simulation curve is shown in Fig. 17. The failure ratio of the fitted curve is 0.55. It can be seen in Fig. 17 that the fitted curve fits well with the measured results.

The calculated results of the model PGPN pile with and without enlarged cemented soil base are shown in Fig. 18. This figure shows that the behavior of the PGPN pile with enlarged cemented soil base was obviously better than that of the PGPN pile without enlarged cemented soil base. Specifically, when an enlarged cemented soil base is set at PGPN pile tip, the load at pile head increased from 37.0 kN to 47.0 kN when the pile head displacement reached 11 mm (0.1*D*, *D* represents pile diameter). Moreover, the pile head load increased from 53.0 kN to 70.6 kN when the pile head displacement reached 40 mm, and the pile head load increased by 33%. When the applied pile head load reached 50 kN, the pile head displacements were 13.0 mm and 31.8 mm, respectively, for the piles with and without enlarged cemented soil base, and the pile head displacement could be decreased by 59.1% by setting an enlarged cemented soil base. The computed results show that the enlarged cemented soil base is effective in promoting the behavior of a short PGPN pile under compression, and the promotion effect becomes more obvious with the application of an increasing pile head load.

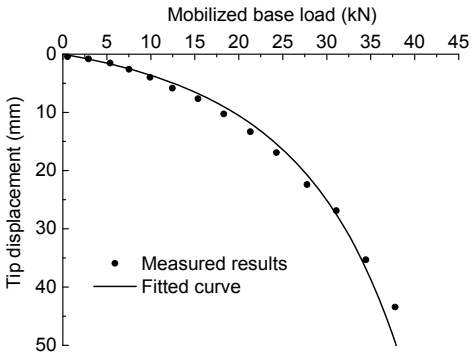

Fig. 17 Fitted curve of the behavior of pile tip

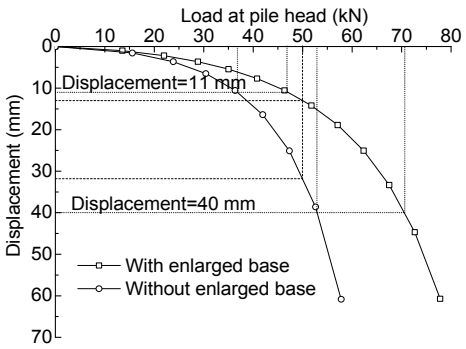

Fig. 18 Calculated results of PGPN pile with and without enlarged cemented soil base

6.2 Comparison of a long PGPN pile

A field test of a long PGPN pile was also used to verify the reliability of the proposed approach in this study, and the properties of the soil at the test site are shown in Table 2. The test pile was a 72-m long PGPN pile, and the core precast pile consisted of pipe piles and nodular piles. Three 800-mm pipe piles with lengths of 15 m, 15 m, and 12 m were connected to two 15-m long 800 (600)-mm nodular piles. The diameter of the drilling hole was 850 mm. The comparisons between the measured and fitted results are shown in Fig. 19. This figure shows that the fitted curve can represent the measured results well when the initial shearing stiffness of the pile-soil interface is enlarged to about 4, 5, 5, 6, 7, 9, 10, and 15 times of the initial calculated values of the soil layers from shallow to deep. Fig. 19 also shows that the respective failure ratios of the soil layers from shallow to deep are 0.7, 0.7, 0.8, 0.8, 0.9, 0.9, 0.9, and 0.98.

The pile tip behavior of the test pile is shown in Fig. 20, which demonstrates that the mobilized base

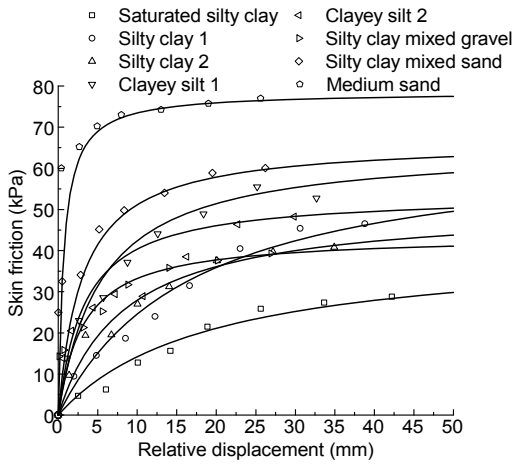

Fig. 19 Comparisons between the measured and fitted results of the relationship between the unit skin friction and relative displacement for different soil layers

Table 2 Soil profiles and properties at the test site

Layer No.	Soil layer	Thickness (m)	γ_{sat} (kN/m^3)	e	IP	IL	Consolidated quick shear		E_s (MPa)	G_s (MPa)	Cone penetration test		q_{ik} (kPa)
							c (kPa)	φ (°)			q_c (MPa)	f_s (kPa)	
1	Clay	5.0	18.4	1.04	19.2	0.75	27.1	12.9	4.70	1.75	0.46	12.99	25
2	Silty clay 1	7.6	17.0	1.46	20.1	1.45	12.1	8.2	3.57	1.34	0.45	8.00	13
3	Silty clay 2	8.4	18.4	1.00	13.0	1.22	12.9	11.4	4.23	1.66	0.79	12.66	20
4	Silty clay 3	7.3	19.0	0.89	16.2	0.62	34.7	17.8	6.70	2.66	1.73	47.70	46
5	Clayey silt 1	4.6	19.0	0.86	7.6	1.16	12.4	30.2	9.84	4.34	6.17	100.3	42
6	Clayey silt 2	24.1	19.0	0.87	8.0	1.16	12.7	29.5	10.6	4.62	4.52	121.6	40
7	Silty clay mixed gravel	7.4	19.6	0.75	13.4	0.43	42.8	20.6	9.02	3.91	–	–	60
8	Silty clay mixed sand	3.2	19.7	0.75	14.7	0.37	43.1	20.5	9.51	4.11	–	–	62
9	Medium sand	7.2	20.1	0.61	–	–	9.9	34.0	12.2	5.17	–	–	78
10	Silty sand	8.2	19.3	0.76	–	–	9.8	32.3	10.1	4.31	–	–	75

γ_{sat}: saturated unit weight; e: void ratio; IP: plasticity index; IL: liquidity index; q_c: cone tip resistance; q_{ik}: standard value of the skin friction of the bored pile

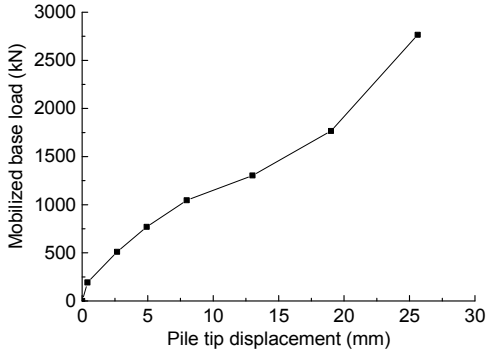

Fig. 20 Pile tip displacement as a function of the mobilized base load

load increases stably with increasing pile tip displacement. This is probably because the permeation of the cement paste makes the base soil brittle compared to the original soil.

Hence, an elastic linear model was used to simulate the base load-displacement response. Moreover, it is important to note that unfortunately, the statistics regarding the pile tip displacement and the mobilized base load after the ultimate mobilized base load was reached were not calculated due to an error in the field test.

The pile base displacement induced by the mobilized base load can also be expressed as

$$P_b = \begin{cases} k_1 S_b, & S_b < S_{bu}, \\ k_1 S_{bu}, & S_b \geq S_{bu}, \end{cases} \quad (15)$$

where k_1 is the compressive rigidity of the interface between the PGPN pile base and the base soil, and S_{bu} is the threshold pile base displacement at which the tip resistance reaches the ultimate value.

The fitted curve of the pile tip behavior based on the measured results is shown in Fig. 21. This figure shows that the fitted line can approximately represent the measured results when k_1=108 kN/mm.

The pile top load and settlement can also be calculated based on the proposed models and parameters selected above. Step 2 in the algorithm process should be modified to be: Consider a small pile base displacement S_b (e.g., 0.1 mm in this study), and calculate the mobilized base load P_b using Eq. (15).

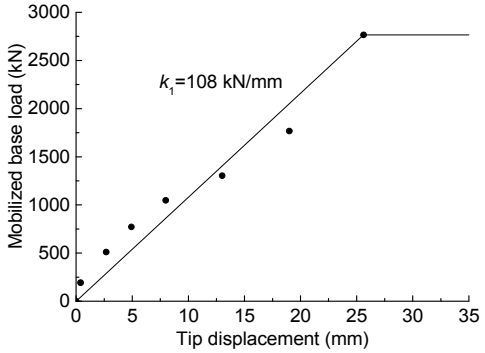

Fig. 21 Comparisons between the fitted and measured results of the relationship between the tip resistance and the base displacement

The comparisons between the calculated and measured results are shown in Fig. 22. Fig. 22 demonstrates that the calculated curve can represent the measured results well, and the calculated ultimate bearing capacity is nearly equal to the measured value. Hence, the calculated value can also be considered to be reliable. The proposed approach is thus shown to be efficient and suitable for the analysis of a long PGPN pile in layered soils.

For a long PGPN pile used in soft soil areas, the entire bearing capacity is supported mainly by the shaft resistance, and the shaft resistance is mainly controlled by the unit skin friction and the pile shaft diameter. The ultimate skin friction of the concrete-cemented soil is much larger than the ultimate skin friction of the cemented soil-soil interface, and the behavior of the PGPN pile can probably be promoted by increasing the diameter of the cemented soil. The cemented soil diameter was therefore enlarged to 900 mm, 1000 mm, and 1100 mm, respectively, and the computed results are shown in Fig. 23.

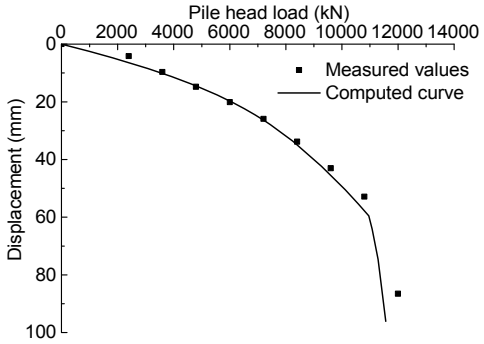

Fig. 22 Comparison between the calculated and measured load-displacement responses for a long PGPN pile

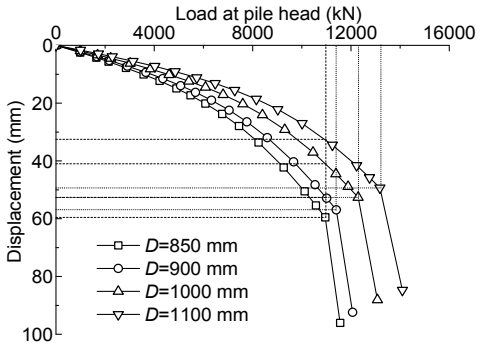

Fig. 23 Calculated load-displacement responses of PGPN pile with different diameters

It can be seen from Fig. 23 that the ultimate bearing capacity of the PGPN pile increased as the diameter of cemented soil increased, while the corresponding pile head displacement decreased with the increasing diameter. The calculated values of the ultimate pile head loads and displacements are listed in Table 3, and the relationship between the cemented soil diameter and ultimate bearing capacity is shown in Fig. 24.

Table 3 Summary of calculated results

Cemented soil diameter (mm)	Ultimate bearing capacity (kN)	Displacement (mm)
850	10 956	59.53
900	11 402	56.90
1000	12 292	52.53
1100	13 181	49.33

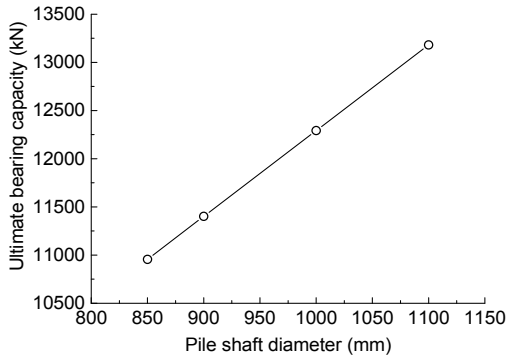

Fig. 24 Relationship between the ultimate bearing capacity and cemented soil diameter

It can be seen from Fig. 24 that the ultimate bearing capacity of the PGPN pile increased almost linearly with the increasing pile diameter as the shaft resistance took up the majority of the entire applied pile head load. The ultimate bearing capacity increased from 10 956 kN to 13 181 kN when the cemented soil diameter increased from 850 mm to 1100 mm, and the bearing capacity increased by 20%. Table 3 shows that the ultimate pile head displacement decreased from 59.53 mm to 49.33 mm when the cemented soil diameter increased from 850 mm to 1100 mm. This is because the axial load along the pile shaft decreases more rapidly with a larger pile shaft diameter.

It can also be seen from Fig. 23 that, with a certain 10 956 kN applied load, the pile head displacements

were 59.5 mm, 52.6 mm, 41.0 mm, and 32.5 mm, respectively, with the cemented soil diameter increasing from 850 mm to 1100 mm. That is, the pile head displacement can be decreased by 45.4% by increasing the cemented soil diameter from 850 mm to 1100 mm. Therefore, the increase of cemented soil diameter can not only increase the ultimate bearing capacity, but also reduce the pile head displacement.

7 Conclusions

This paper presents a simplified approach for the analysis of the behavior of a single PGPN pile embedded in layered soils. An elastic-failure model, based on shear test results, was used to describe the behavior of the concrete-cemented soil interface. A hyperbolic nonlinear model was used to describe the relationship between the skin friction and the relative displacement between cemented soil and soil. A linear model and a nonlinear model that considers the reduction of the shearing stiffness were used to simulate the pile tip load-displacement responses in the field and model tests, respectively. Comparisons between the calculated and measured load-displacement responses demonstrated the reliability of the proposed approach. The proposed approach is considered to be efficient and suitable for the analysis of a single PGPN pile embedded in layered soils by considering the influence of the cement paste injection, the varying pile shaft modulus, and the existence of the enlarged pile base. Moreover, based on the calculated results, the enlarged cemented soil base is considered to be effective in promoting the behavior of a short PGPN pile, and an increase in the diameter of cemented soil is efficient in promoting the compressive bearing capacity of a long PGPN pile. This simplified approach can also be used for the analysis of similar precast pile-cemented soil composite piles which have two interfaces of the pile shaft.

References

Ai, Z.Y., Han, J., 2009. Boundary element analysis of axially loaded piles embedded in a multi-layered soil. *Computers and Geotechnics*, **36**(3):427-434. http://dx.doi.org/10.1016/j.compgeo.2008.06.001

Clough, G.W., Duncan, J.M., 1971. Finite element analysis of retaining wall behavior. *Journal of the Soil Mechanics and Foundation Division*, **97**(SM12):1657-1673.

Comodromos, E.M., Papadopoulou, M.C., Rentzeperis, I.K., 2009. Pile foundation analysis and design using experimental data and 3-D numerical analysis. *Computers and Geotechnics*, **36**(5):819-836. http://dx.doi.org/10.1016/j.compgeo.2009.01.011

Duncan, J.M., Chang, C.Y., 1970. Nonlinear analysis of stress and strain in soils. *Journal of the Soil Mechanics and Foundation Division*, **96**(5):1629-1653.

Frank, R., Zhao, S.R., 1982. Estimation par les Parametres Pressiometriques de L'enfoncement sous Charge Axiale de Pieux Fores Dans des Sols Fins. Bull Liaison Lab Ponts Chauss (in French).

Han, J., Ye, S.L., 2006. A field study on the behavior of micropiles in clay under compression or tension. *Canadian Geotechnical Journal*, **43**(1):19-29. http://dx.doi.org/10.1139/t05-089

Horiguchi, T., Karkee, M.B., 1995. Load tests on bored PHC nodular piles in different ground conditions and the bearing capacity based on simple soil parameters. *Proceedings of Technical Report of Japanese Architectural Society*, **1**:89-94 (in Japanese).

Karkee, M.B., Kanai, S., Horiguchi, T., 1998. Quality assurance in bored PHC nodular piles through control of design capacity based on loading test data. Proceedings of the 7th International Conference and Exhibition, Piling and Deep Foundations, **1**(24):1-9.

Kondner, R.L., 1963. Hyperbolic stress-strain response: cohesive soils. *Journal of Geotechnical Engineering Division*, **89**(1):115-143.

Kraft, L.M.Jr., Ray, R.P., Kagawa, T., 1981. Theoretical *t-z* curves. *Journal of Geotechnical Engineering Division*, **107**(11):1543-1561.

Kulhawy, F.H., 1984. Limiting tip and side resistance: fact or fallacy? Proceeding of Analysis and Design of Pile Foundations, p.80-98.

Lee, K.M., Xiao, Z.R., 2001. A simplified nonlinear approach for pile group settlement analysis in multilayered soils. *Canadian Geotechnical Journal*, **38**(5):1063-1080. http://dx.doi.org/10.1139/t01-034

Mandolini, A., Viggiani, C., 1997. Settlement of piled foundations. *Geotechnique*, **47**(4):791-816. http://dx.doi.org/10.1680/geot.1997.47.4.791

Randolph, M.F., Wroth, C.P., 1978. Analysis of deformation of vertically loaded pile. *Journal of Geotechnical Engineering Division*, **104**(12):1465-1488.

Randolph, M.F., Wroth, C.P., 1979. An analysis of the vertical deformation of pile groups. *Geotechnique*, **29**(4):423-439. http://dx.doi.org/10.1680/geot.1979.29.4.423

Said, I., De, G.V., Frank, R., 2009. Axisymmetric finite element analysis of pile loading tests. *Computers and Geotechnics*, **36**(1-2):6-19. http://dx.doi.org/10.1016/j.compgeo.2008.02.011

Sheng, D.C., Eigenbrod, K.D., Wriggers, P., 2005. Finite element analysis of pile installation using large-slip frictional contact. *Computers and Geotechnics*, **32**(1):17-26.

http://dx.doi.org/10.1016/j.compgeo.2004.10.004

Zhou, J.J., Wang, K.H., Gong, X.N., *et al*., 2013. Bearing capacity and load transfer mechanism of a static drill rooted nodular pile in soft soil areas. *Journal of Zhejiang University-SCIENCE A (Applied Physics & Engineering)*, **14**(10):705-719.
http://dx.doi.org/10.1631/jzus.A1300139

Zhou, J.J., Gong, X.N., Wang, K.H., *et al*., 2015. A field study on the behavior of static drill rooted nodular piles with caps under compression. *Journal of Zhejiang University-SCIENCE A (Applied Physics & Engineering)*, **16**(12):951-963.
http://dx.doi.org/10.1631/jzus.A1500168

Zhou, J.J., Gong, X.N., Wang, K.H., *et al*., 2016. A model test on the behavior of a static drill rooted nodular pile under compression. *Marine Georesources & Geotechnology*, **34**(3):293-301.
http://dx.doi.org/10.1080/1064119X.2015.1012313

Zhou, J.J., Gong, X.N., Wang, K.H., *et al*., 2017. Testing and modeling the behavior of pre-bored grouting planted piles under compression and tension. *Acta Geotechnica*, **12**(5):1061-1075.
http://dx.doi.org/10.1007/s11440-017-0540-6

中文概要

题　目： 一种静钻根植竹节桩非线性简化沉降计算方法

目　的： 静钻根植竹节桩是一种由预制桩和水泥土组成的组合桩基，其桩身具有预制桩-水泥土和水泥土-桩周土体两个接触面。本文以桩土接触面剪切试验、模型试验和现场试验数据为基础，提出一种静钻根植竹节桩简化沉降计算方法，为静钻根植竹节桩的沉降计算提供依据；并通过所提出的简化计算方法对静钻根植竹节桩桩端水泥土扩大头以及桩周水泥土直径对静钻根植竹节桩承载性能的影响进行研究。

创新点： 1. 通过剪切试验对预制桩-水泥土接触面的剪切性能进行研究，得到接触面侧摩阻力与相对位移的关系；2. 建立同时考虑预制桩-水泥土接触面和水泥土-桩周土体接触面作用的静钻根植竹节桩简化沉降计算方法。

方　法： 1. 通过桩土接触面剪切试验，得到预制桩-水泥土接触面摩擦模型；2. 通过对模型试验结果的分析，得到水泥土-桩周土体接触面摩擦模型；3. 根据试验结果编写静钻根植竹节桩沉降计算程序，通过与试验结果的比较验证所提计算方法的可靠性；4. 通过提出的静钻根植竹节桩简化计算方法对静钻根植竹节桩承载力影响因素进行分析与研究。

结　论： 1. 预制桩-水泥土接触面摩擦性能远优于水泥土-桩周土体接触面摩擦性能；2. 由于水泥浆的渗透作用，水泥土-桩周土体接触面的初始剪切刚度有所提高；3. 所提出的计算方法能够有效地计算出静钻根植竹节桩单桩在成层土体中的荷载位移关系曲线；4. 桩端水泥土扩大头能够有效地提高静钻根植竹节桩桩端承载性能，并且增加桩周水泥土直径能够提高静钻根植竹节桩承载性能。

关键词： 组合桩基；预制桩-水泥土-桩周土体接触面；桩土接触面初始剪切刚度；弹性-破坏模型；双曲线模型；沉降计算